

Charge transfer processes in low-energy Na^{+}-Na collisions

Cheng-Cheng Jiang(蒋承呈), Xiao-Xia Wang(王小霞), Kun Wang(王堃), Yi-Zhi Qu(屈一至), Jian-Guo Wang(王建国), Xia Li(李侠), Li Ma(马丽), and Robert J. Buenker

Citation: Chin. Phys. B, 2026, 35 (**4**): 043402. DOI: 10.1088/1674-1056/ae15f0
http://cpb.iphy.ac.cn; http://iopscience.iop.org/cpb

What follows is a list of articles you may be interested in

Single electron capture in low- and intermediate-energy collisions of $Si^{3,4+}$ with He

Yingzhou Li(李英卓), Yadong Liu(刘亚东), Yueying Qi(祁月盈), Ling Liu(刘玲), Yizhi Qu(屈一至), and Jianguo Wang(王建国)

Chin. Phys. B, 2026, 35 (**1**): 013401. DOI: 10.1088/1674-1056/ae15f4

Electron capture and excitation in intermediate-energy He^{2+}-H(1s,2s) collisions

Yadong Liu(刘亚东), Congcong Jia(贾聪聪), Mingxuan Ma(马茗萱), Xiang Gao(高翔), Ling Liu(刘玲), Yong Wu(吴勇), Xiangjun Chen(陈向军), and Jianguo Wang(王建国)

Chin. Phys. B, 2024, 33 (**8**): 083401. DOI: 10.1088/1674-1056/ad5322

A theoretical study of fragmentation dynamics of water dimer by proton impact

Zhi-Ping Wang(王志萍), Xue-Fen Xu(许雪芬), Feng-Shou Zhang(张丰收), and Xu Wang(王旭)

Chin. Phys. B, 2023, 32 (**3**): 033401. DOI: 10.1088/1674-1056/ac8340

Electron excitation processes in low energy collisions of hydrogen-helium atoms

Kun Wang(王堃), Chuan Dong(董川), Yi-Zhi Qu(屈一至), Ling Liu(刘玲), Yong Wu(吴勇),Xu-Hai Hong(洪许海), and Robert J. Buenker

Chin. Phys. B, 2022, 31 (**12**): 123401. DOI: 10.1088/1674-1056/aca14c

Charge transfer in low-energy collisions ofBe^{3+} and B^{4+} ions with He

Kun Wang(王堃), Yi-Zhi Qu(屈一至), Chun-Hua Liu(刘春华), Ling Liu(刘玲), Yong Wu(吴勇), H P Liebermann, Robert J. Buenker

Chin. Phys. B, 2020, 29 (**9**): 093401. DOI: 10.1088/1674-1056/aba276

Charge transfer processes in low-energy Na^+–Na collisions

Cheng-Cheng Jiang(蒋承呈)[1], Xiao-Xia Wang(王小霞)[1,†], Kun Wang(王堃)[2], Yi-Zhi Qu(屈一至)[3], Jian-Guo Wang(王建国)[4], Xia Li(李侠)[1], Li Ma(马丽)[1], and Robert J. Buenker[5]

[1] *College of Physics, Chengdu University of Technology, Chengdu* 610059, *China*
[2] *Institute of Environmental Science, Shanxi University, Taiyuan* 030006, *China*
[3] *College of Material Sciences and Optoelectronic Technology, University of Chinese Academy of Sciences, Beijing* 100049, *China*
[4] *Data Center for High Energy Density Physics, Institute of Applied Physics and Computational Mathematics, Beijing* 100088, *China*
[5] *Fachbereich C-Mathematik und Naturwissenschaften, Bergische Universitat Wuppertal, D-*42097 *Wuppertal, Germany*

(Received 7 August 2025; revised manuscript received 11 October 2025; accepted manuscript online 22 October 2025)

A comprehensive theoretical study of resonant and non-resonant charge transfer processes in the homonuclear Na^+ + Na(3s) collision system is provided. The electronic structure of the quasi-molecular system is calculated using the multireference single- and double-excitation configuration interaction (MRD-CI) method under both one-electron (OEM) and thirteen-electron (TEM) models. The radial and rotational coupling matrix elements are obtained with careful inclusion of electron translation factors (ETFs). Based on these data, fully quantum-mechanical scattering calculations were performed using the fully quantum-mechanical molecular orbital close-coupling (QMOCC) method to derive state-selective and total cross sections for electron capture over a broad energy range (0.2–5600 eV/amu). The calculated resonant charge-transfer cross sections show excellent agreement with available theoretical and experimental results. Non-resonant processes, which involve electron capture into excited states of Na^+, are found to become increasingly important above several keV/amu. This work provides the first theoretical predictions for non-resonant state-selective cross sections in this system, offering a valuable reference for future experimental and theoretical studies in atomic collision physics.

Keywords: charge transfer, resonant and non-resonant processes, QMOCC

PACS: 34.70.+e, 34.20.–b

DOI: 10.1088/1674-1056/ae15f0 **CSTR:** 32038.14.CPB.ae15f0

1. Introduction

Charge transfer plays a fundamental role across a wide range of disciplines, including plasma physics and astrophysics.[1] In plasma physics, detailed investigations of charge transfer processes involving Na^+ ions offer valuable insights into the underlying reaction mechanisms observed in high-temperature guided ion beam experiments.[2] These findings facilitate a more accurate incorporation of metal–atom reactions into plasma modeling, particularly enabling the description of kinetic energy ranges relevant to meteor ablation phenomena. Moreover, understanding charge transfer is essential for interpreting ion dynamics, energy transport, and neutral beam injection phenomena in plasma environments.[3] In astrophysics, charge transfer processes are crucial for interpreting the intensity and spatial distribution of sodium spectral lines observed in astronomical spectra, thereby contributing valuable information for the modeling of diverse celestial environments.[4] In particular, investigations into charge transfer between Jupiter's magnetosphere and volcanic ejecta from its moon Io are essential for elucidating the morphological and kinematical structures of sodium clouds in the Jovian system.[5]

Because of the applications mentioned above, considerable early efforts have been devoted to investigating the charge transfer processes in Na^+–Na collisions. In 1960 and 1969, Bukhteev *et al.*[6] and Daley *et al.*[7] experimentally measured the charge transfer cross sections for Na^+–Na collisions over the energy ranges of 150–2000 eV (6.5–87 eV/amu) and 400–30000 eV (17.4–1305 eV/amu), respectively. These measurements were further extended by Pivovar *et al.*[8] and Rutherford *et al.*[9] (1972), the study covered the energy ranges of 30–155 keV (1304–6742 eV/amu) and 40–500 eV (1.7–21.7 eV/amu). On the theoretical side, Sakabe *et al.*[10] (1991) employed the impact parameter and close coupling (IPCC) method to calculate charge transfer cross sections over a wide energy range from 3 eV to 218 keV (0.13–9482 eV/amu). Subsequently, Copeland *et al.*[11] (1997) applied the impact parameter and treatment of Firsov (IPTF) to calculate cross sections corresponding to collision velocities ranging from 10^6 cm/s to 10^8 cm/s (0.5–5223 eV/amu). With further advancements in theoretical modeling, Thomsen *et al.*[12] (1998) utilized the atomic orbital close-coupling (AOCC) method to calculate charge transfer cross sections across a broad energy range of 57.5 eV–207 keV (2.5–9000 eV/amu).

Among previous studies, the theoretical results of Sakabe *et al.*[10] exhibit good agreement with the experimental measurements of Daley *et al.*[7] in the overlapping energy region.

†Corresponding author. E-mail: wangxx@cdut.edu.cn

© 2026 Chinese Physical Society and IOP Publishing Ltd. All rights, including for text and data mining, AI training, and similar technologies, are reserved.

The AOCC calculations of Thomsen *et al.*[12] and experiments from Pivovar *et al.*[8] and Rutherford *et al.*[9] tend to yield systematically higher cross sections than those of Sakabe *et al.*[10] To the contrary, the measurements by Bukhteev *et al.*[6] and IPTF calculations by Copeland *et al.*[11] are approximately 25% and 50% lower, respectively, than Sakabe's theoretical values. Despite these extensive efforts, discrepancies persist, particularly in the resonant charge transfer cross sections below 1 keV/amu. Moreover, studies focusing on non-resonant charge transfer processes remain limited. These issues highlight the necessity for further high-precision and systematic theoretical investigations to achieve a more complete and consistent understanding of Na^+–Na charge transfer dynamics.

In this work, charge transfer processes in the homonuclear collision system $Na^+ + Na$ are systematically studied, with particular attention given to both resonant and non-resonant channels. The resonant charge transfer corresponds to a case of symmetric resonance, where the initial and final states of the system are identical. In contrast, non-resonant processes involve electron capture into excited states of the incident Na^+ ion. The present study aims to provide a detailed theoretical investigation of these charge transfer processes, including:

Resonant charge transfer: $Na^+(2p^6) + Na(2p^6 3s) \rightarrow Na(2p^6 3s) + Na^+(2p^6)$;

Non-resonant charge transfer: $Na^+(2p^6) + Na(2p^6 3s) \rightarrow Na[(2p^6)3p, 3d, 4s, 4p)] + Na^+(2p^6)$.

The *ab initio* multireference single- and double-excitation configuration interaction (MRD-CI) quantum chemistry package[13–15] was employed to calculate the adiabatic potential energy curves over an internuclear distance range of 1–50 a.u. This package also obtained the radial and rotational coupling matrix elements. To ensure Galilean invariance, the electron translation factors (ETFs)[16] were incorporated into the electronic structure calculations. Based on these calculations, the resonant and non-resonant charge transfer processes in the $Na^+ + Na(3s)$ collision system are then investigated using the fully quantum-mechanical molecular orbital close-coupling (QMOCC) method,[17–19] covering the collision energy ranges of 0.6–5600 eV/amu and 0.2–5600 eV/amu, respectively. Atomic units are used throughout unless otherwise stated.

2. Theoretical method

The charge-transfer cross sections for $Na^+ + Na(3s)$ collisions were calculated using the QMOCC method, as detailed in previous works.[17–19] For low-energy collisions, the electronic wave function could be replaced with its adiabatic counterpart in the perturbed stationary state (PSS) framework.[19–21] Under the Born–Oppenheimer approximation, the total wavefunction of the collision system can be well described by adiabatic wavefunctions $\psi_i(\boldsymbol{R}, \boldsymbol{r})$

$$\Psi(\boldsymbol{R}, \boldsymbol{r}) = \sum_i F_i(\boldsymbol{R})\, \psi_i(\boldsymbol{R}, \boldsymbol{r}), \tag{1}$$

where $\boldsymbol{R}$ represents the internuclear distance, $\boldsymbol{r}$ is the electron position vector taken with respect to the center of mass of the nuclei. The summation over i is limited to a subset of the complete set of adiabatic states $\{\psi_i\}$. Since each state in the asymptotic region corresponds to an atomic state, these states are referred to as channel states. After the partial wave expansion for the channel function

$$F_j(\boldsymbol{R}) = R^{-1} \sum_{J=0} f_j^J(\boldsymbol{R})\, D^J_{M\lambda_j}(\theta, \varphi), \tag{2}$$

where $D^J_{M\lambda_j}$ is the total angular wavefunction, the radial function $f^J(R)$, satisfying the differential equation in rotating coordinates, is obtained

$$\begin{aligned} &\left[\frac{\mathrm{d}^2}{\mathrm{d}R^2} - \frac{J(J+1) - \lambda^2}{R^2} - 2\mu(u(R) - E)\right] f^J(R) \\ &= \left(V^{\mathrm{R}}(R) + V^{\mathrm{C}}(R)\right) f^J(R). \end{aligned} \tag{3}$$

Here μ denotes the reduced mass, and u corresponds to the diagonal adiabatic potential matrix. $J(J+1)$ and λ are eigenvalues of the total system angular momentum $\hat{J}^2$ and the electronic angular momentum $\hat{L}_z$, while E represents the total energy. The radial and rotational coupling matrices, designated as V^{R} and V^{C}, respectively, satisfy the following standard forms:

$$\begin{aligned} V^{\mathrm{R}}_{ij}(R) = \Bigg[&\langle i| - \frac{\partial^2}{\partial R^2} + \frac{L_x^2 + L_y^2}{R^2} |j\rangle \\ &- 2\langle i| \frac{\partial}{\partial R} |j\rangle \frac{\partial}{\partial R}\Bigg] \delta_{\lambda_i, \lambda_j}, \end{aligned} \tag{4a}$$

$$\begin{aligned} V^{\mathrm{C}}_{ij}(R) = &-2\delta_{\lambda_i, \lambda_j + 1} \left[(J - \lambda_i)(J + \lambda_i + 1)\right]^{1/2} \frac{\langle i| \mathrm{i}L_y |j\rangle}{R^2} \\ &+ 2\delta_{\lambda_i, \lambda_j - 1} \left[(J + \lambda_i)(J - \lambda_i + 1)\right]^{1/2} \frac{\langle i| \mathrm{i}L_y |j\rangle}{R^2}. \end{aligned} \tag{4b}$$

The coupling matrices contribute to electron exchange between states of the same (V^{R}_{ij}) or different (V^{C}_{ij}) symmetry. The states $\langle i|$ and $|j\rangle$ denote the adiabatic electronic wavefunctions $\langle \psi_i|$ and $|\psi_j\rangle$, respectively. The most significant term in radial coupling is $A^{\mathrm{R}}_{ij} = \langle i| \frac{\partial}{\partial R} |j\rangle$, which is typically evaluated using finite-difference methods. $A^{\theta}_{ij} = \langle i| \mathrm{i}L_y |j\rangle$ represents the rotational coupling matrix elements.

Due to the near-singular behavior of the radial couplings near long-range avoided crossings, it is often necessary to perform a diabatic transformation of the radial wavefunction

$$f^J(R) = C g^J(R), \quad \frac{\mathrm{d}C}{\mathrm{d}R} + A^{\mathrm{R}} C = 0. \tag{5}$$

The matrix C is a unitary transformation obtained by solving the corresponding differential equation. In the case of a complete basis, the diabatic radial coupling matrix elements vanish. Although obtaining a truly complete basis is challenging

in practice, the large electronic basis employed in the present study is expected to provide an accurate diabatic representation. Consequently, the radial coupling function becomes well-behaved under this transformation

$$\left[\frac{\mathrm{d}^2}{\mathrm{d}R^2}-\frac{J(J+1)-\lambda^2}{R^2}+2\mu E\right]g^J_\gamma=2\mu\sum_{\gamma'}U_{\gamma,\gamma'}(R)g^J_{\gamma'},$$
$$U_{\gamma,\gamma'}(R)\equiv[C(u-P)C^{-1}]_{\gamma\gamma'}. \tag{6}$$

$U(R)$ denotes the diabatic potential matrix with off-diagonal elements facilitating charge transfer. P is the rotational coupling matrix with elements for the diabatic states

$$P_{ij}=\mp\frac{1}{\mu R^2}[(J\mp\lambda_i)(J\pm\lambda_i+1)]^{1/2}A^\theta_{ij}\delta(\lambda_i,\lambda_j\mp1)]. \tag{7}$$

These equations are solved using the multichannel log-derivative method developed by Johnson.[22] In the asymptotic limit, the ion-neutral and Coulomb channel coefficients are fitted to spherical Bessel functions and Coulomb functions, respectively, allowing us to extract the K matrix.

The Na^+–Na collision is a symmetric system involving identical nuclei, whose wavefunction is composed of two dynamically uncoupled forms: gerade (g) and ungerade (u) symmetry. The gerade wavefunction is symmetric with respect to the exchange of nuclei, while the ungerade wavefunction is antisymmetric. The radial differential equations must be solved separately for both gerade and ungerade states. Then the corresponding scattering matrices S can be obtained accordingly

$$S^{\mathrm{g,u}}_{ij,J}=\frac{I+\mathrm{i}K^{\mathrm{g,u}}_{ij,J}}{I-\mathrm{i}K^{\mathrm{g,u}}_{ij,J}}. \tag{8}$$

The charge transfer occurring between dynamically uncoupled gerade and ungerade symmetry is driven by the interference of scattering amplitudes, which can be expressed in the standard form from Bransden and McDowell[21]

$$f^{\mathrm{g,u}}_{ij}(\theta)=\frac{1}{2\mathrm{i}k_i}\sum_{J=0}^{\infty}(2J+1)(S^{\mathrm{g,u}}_{ij,J}-\delta_{ij})P_J(\cos\theta), \tag{9}$$

where k_i is the initial center-of-mass momentum, J is the total angular momentum quantum number, and $P_J(\cos\theta)$ denotes the Legendre polynomial of order J. The differential cross section for charge transfer is then given by

$$\frac{\mathrm{d}\sigma^{\mathrm{ct}}}{\mathrm{d}\Omega}=\frac{1}{4k_i^2}\left(\sum_{J=0}^{\infty}(2J+1)S^{\mathrm{ct}}_{ij,J}P_J(\cos\theta)\right)^2, \tag{10}$$

where $S^{\mathrm{ct}}_{ij,J}=\frac{1}{2}(S^{\mathrm{g}}_{ij,J}-S^{\mathrm{u}}_{ij,J})$. The case of $i=j$ corresponds to resonant charge transfer processes, whereas $i\neq j$ indicates non-resonant charge transfer. By integrating the differential cross section over the entire solid angle Ω, the integral cross section for the resonant charge transfer process is obtained as

$$\sigma^{\mathrm{ct}}=\frac{\pi}{k_i^2}\sum_{J=0}^{\infty}(2J+1)\left|S^{\mathrm{ct}}_{ij,J}\right|^2. \tag{11}$$

3. Results and discussion

3.1. Molecular structure

In this study, the electronic structures of the Na^+–Na system are calculated over an internuclear distance range of 1.0–50.0 a.u. using the *ab initio* MRD-CI quantum chemistry package. To investigate the influence of the $n=2$ subshell, two models are employed: the one-electron model (OEM) and the thirteen-electron model (TEM). In the OEM, electrons in the $n=1$ and $n=2$ shells are described using the LANL08 effective core potential (ECP).[23] The 3s valence electron, which is the only active electron in this model, is treated with a [3s, 3p] Gaussian-type basis set,[24] further augmented with additional (2s, 2p, 2d) diffuse functions to improve the description of long-range interactions. In the TEM, the $n=2$ shell is explicitly included in the active space, while the 1s electrons are described by the CRENBL[25] effective core potential. The remaining electrons are represented using a [6s, 4p] basis set, also augmented with (2s, 2p, 2d) diffuse functions. In this model, the 2s orbital is frozen, resulting in thirteen active electrons occupying the 2p and 3s orbitals.

For both models of the Na^+–Na(3s) collision system, five $^2\Sigma^+$ states and three $^2\Pi$ states, including both gerade and ungerade symmetries, are considered in the calculations. As shown in Table 1, the energy discrepancies (error) between the present MRD-CI results and the experimental data reported in the NIST database[26] are less than 0.1 eV. This close agreement provides a reliable foundation for the subsequent scattering calculations.

Table 1. Asymptotic atomic energies of the Na_2^+ molecular ion states compared with NIST experimental data.

Molecular states	Asymptotic atomic states	Energy (eV)				
		NIST	MRDCI		Error	
			OEM	TEM	OEM	TEM
$1\,^2\Sigma^+_{g/u}$	Na^++Na ($2p^6 3s\ ^2S$)	0.000	0.000	0.000	0.000	0.000
$2\,^2\Sigma^+_{g/u}$, $1\,^2\Pi_{g/u}$	Na^++Na ($2p^6 3p\ ^2P^\circ$)	2.102	2.094	2.175	–0.008	0.073
$3\,^2\Sigma^+_{g/u}$	Na^++Na ($2p^6 4s\ ^2S$)	3.191	3.145	3.246	–0.046	0.055
$4\,^2\Sigma^+_{g/u}$, $2\,^2\Pi_{g/u}$	Na^++Na ($2p^6 3d\ ^2D$)	3.617	3.587	3.698	–0.030	0.081
$5\,^2\Sigma^+_{g/u}$, $3\,^2\Pi_{g/u}$	Na^++Na ($2p^6 4p\ ^2P^\circ$)	3.753	3.785	3.837	0.032	0.084

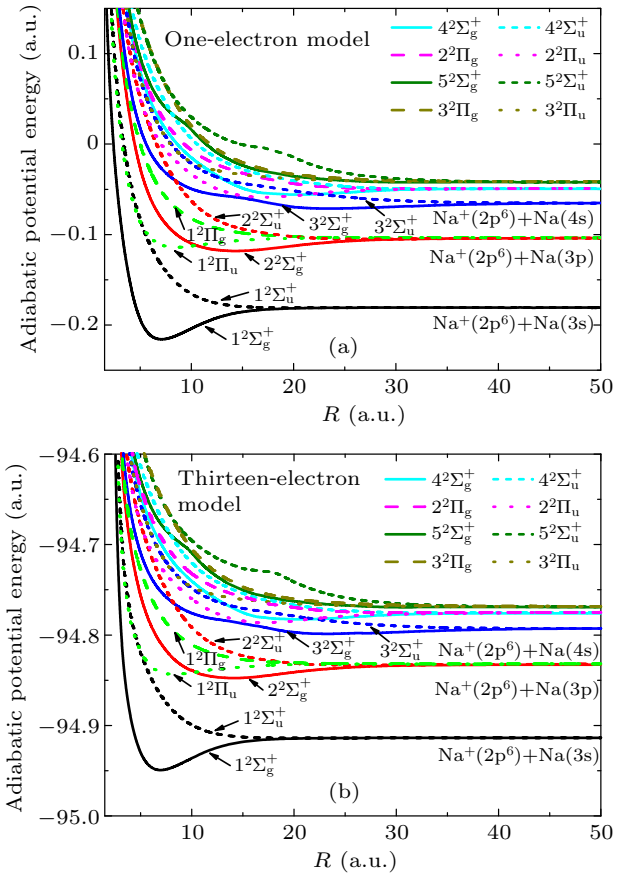


Fig. 1. Adiabatic potential energy curves of the Na^+–Na system in both gerade and ungerade states, calculated using (a) the one-electron model (OEM) and (b) the thirteen-electron model (TEM).

Figure 1 shows the adiabatic potential energy curves of the Na^+–Na system for both gerade and ungerade states, obtained from the one-electron model [Fig. 1(a)] and the thirteen-electron model [Fig. 1(b)]. The potential energy curves obtained from both models exhibit generally consistent trends, indicating that the simplified one-electron approximation captures the essential features of the interaction potential in this system. The similarity between the two models also suggests that the contributions from inner-shell electrons have a limited impact on the overall potential landscape. Among the calculated molecular states, several molecular state pairs correspond to the same asymptotic atomic states, such as ($2\,^2\Sigma_g^+$, $2\,^2\Sigma_u^+$) and ($1\,^2\Pi_g$, $1\,^2\Pi_u$). On one hand, the energy separations between the initial states ($1\,^2\Sigma_g^+$ and $1\,^2\Sigma_u^+$) and other molecular states exceed 2.1 eV; on the other hand, these initial states exhibit no significant coupling with the neighboring states. Consequently, the resonant charge transfer process between $1\,^2\Sigma_g^+$ and $1\,^2\Sigma_u^+$ is expected to play a dominant role in the overall charge transfer dynamics. Furthermore, the potential energy curves do not exhibit any obvious avoided crossings, which typically signal strong non-adiabatic interactions. The absence of such features suggests that the nonresonant charge transfer processes proceed via long-range, weak couplings and are most likely governed by a Demkov-type mechanism.[27,28] In this mechanism, charge transfer occurs through diabatic transitions facilitated by small but long-range radial coupling elements, rather than through Landau–Zener-type[29] processes that typically involve strong avoided crossings.

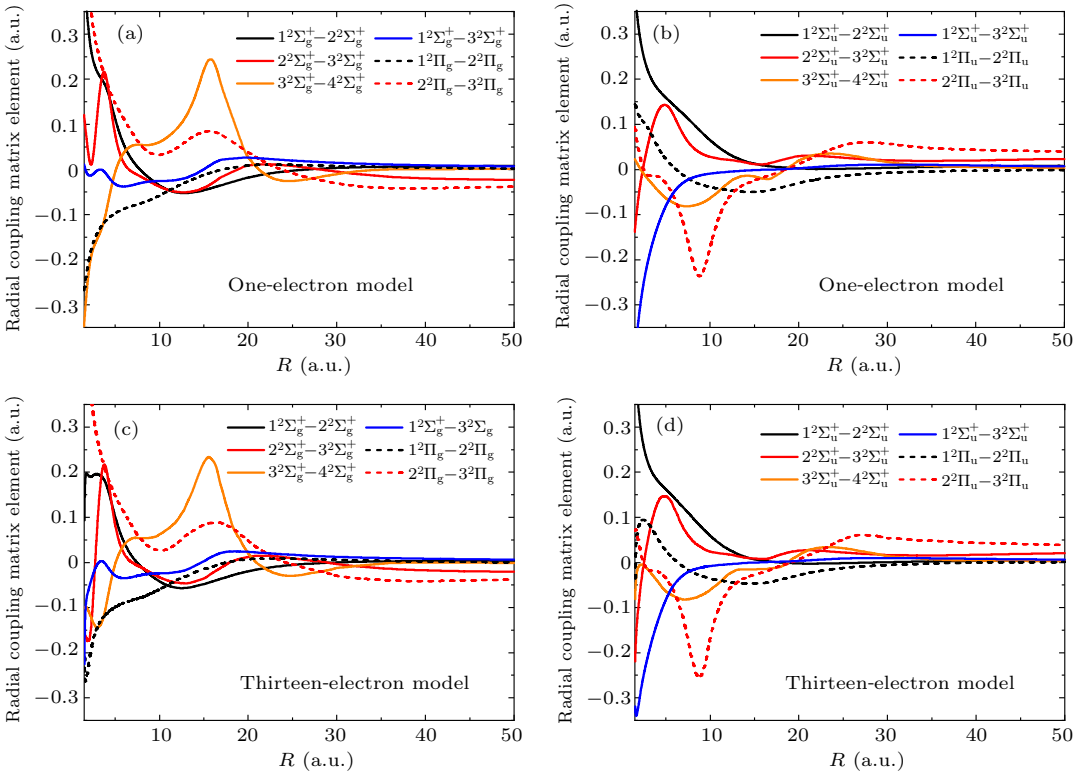


Fig. 2. Radial coupling matrix elements of the Na_2^+ molecular ion under one-electron and thirteen-electron models.

In the absence of an obvious avoided crossing in the potential energy curves, non-resonant charge transfer generally occurs between the initial channel and its neighboring channels. In this case, the radial and rotational couplings between adjacent channels play a particularly significant role. Figure 2 displays the radial coupling matrix elements for both the one-electron model and the thirteen-electron model with electron translation factors (ETFs) taken into account in gerade and ungerade symmetries, respectively. It is found that the coupling matrix elements calculated using both the one-electron model and the thirteen-electron model are in close agreement; for example, the peak positions of the couplings between $3\,^2\Sigma_g^+$ and $4\,^2\Sigma_g^+$ occur at approximately 15.8 a.u., and between $2\,^2\Pi_u$ and $3\,^2\Pi_u$ at around 8.8 a.u. As shown clearly in Fig. 2, the radial couplings among these states exhibit relatively weak long-range interactions, which can play a crucial role in non-resonant charge transfer processes. In particular, the [Na^+(2p)+Na(3p); $2\,^2\Sigma^+/1\,^2\Pi$] states are energetically closest to the initial channel [Na^+(2p)+Na(3s); $1\,^2\Sigma^+$], and their radial couplings display broad and shallow peaks. This indicates that the electron is most likely to transfer to the Na(3p) state, and these two couplings serve as the primary gateways for charge-transfer flux from the initial to the exit channels.

During the collision process, the electron may be captured by the $^2\Pi$ state through rotational coupling, which is also considered in the present calculation. Some representative rotational coupling matrix elements are shown in Fig. 3. The couplings between states with the same atomic configurations, such as $2\,^2\Sigma^+$–$1\,^2\Pi$ and $4\,^2\Sigma^+$–$2\,^2\Pi$, approach a value of 1 at large internuclear distances in both gerade and ungerade symmetries. In particular, a notable long-range rotational coupling between $1\,^2\Sigma_g^+$ and $1\,^2\Pi_g$ will ensure a non-negligible electron flux into this channel even at low collision energies, thereby significantly contributing to the non-resonant charge transfer processes. As illustrated in Figs. 3(b) and 3(d), strong rotational coupling between $1\,^2\Sigma_u^+$ and $1^2\Pi_u$ plays a critical role in determining the state-selective population observed in the scattering cross sections. These rotational couplings provide essential pathways for electron capture beyond the radial coupling mechanisms and must be carefully considered for an accurate description of the collision dynamics.

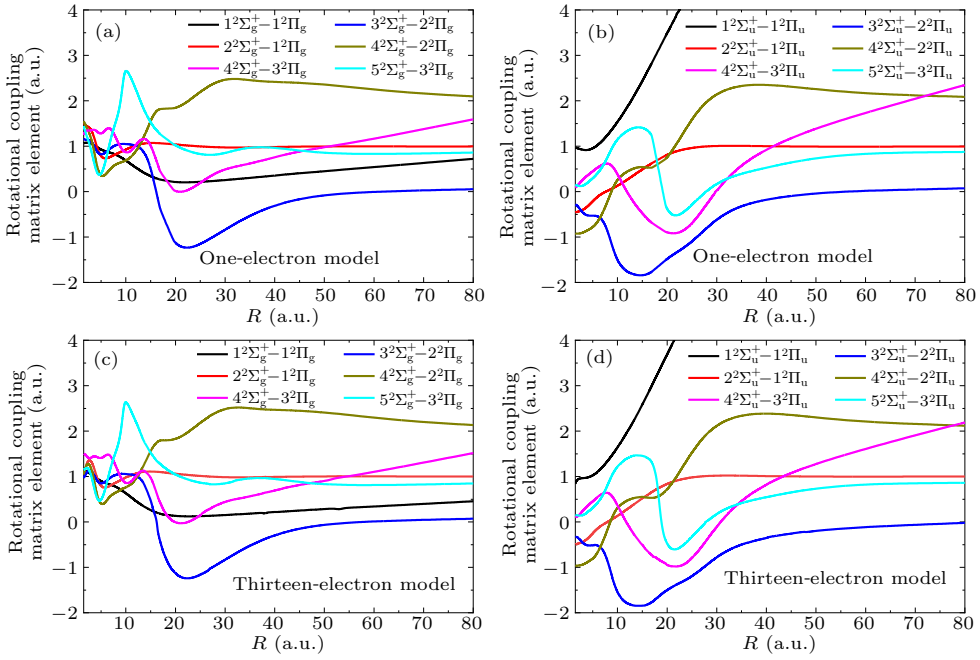


Fig. 3. Rotational coupling matrix elements of the Na_2^+ molecular ion under the one-electron model and the thirteen-electron model.

3.2. Charge transfer cross sections

3.2.1. Resonant charge transfer

Based on the electronic structure of Na_2^+ quasi-molecular system, the QMOCC method was employed to obtain the resonant charge transfer cross sections. The results, presented in Fig. 4 for the energy range of 0.6 eV/amu to 5600 eV/amu, are thoroughly compared with available experimental and theoretical data. The present QMOCC results obtained from the one-electron model and the thirteen-electron model have good agreement in the overall energy region, with discrepancies remaining below 5%. In low-energy collisions, the resonant charge transfer cross sections are sensitive to the electronic structure. Therefore, the discrepancies observed between the two models can be attributed to the small differences in potential energy curves and coupling matrix elements between these two models.

The present QMOCC results show good agreement with the 26-state two-center atomic orbital close-coupling (AOCC)

calculations reported by Thomsen *et al.*[12] within the energy range of 8 eV/amu to 2 keV/amu. Furthermore, the present data connect well with the experimental measurements of Rutherford *et al.*[9] at energies below 10 eV/amu, as well as those of Pivovar *et al.*[8] in the range of 1.3–5.6 keV/amu. In the coincident region with AOCC, the discrepancies between the present QMOCC results and the AOCC calculations remain within 10%. The electron translational factors (ETFs) are also included in the scattering equations in the AOCC method, which are expected to be important for collision energies above 1 keV/amu.[30] For collision energies below 8 eV/amu, the AOCC calculations yield smaller cross sections than the QMOCC results, which may be attributed to the use of a one-electron model and the impact parameter approximation in the work of Thomsen *et al.*[12] For energies above 2.5 keV/amu, the QMOCC results exceed the AOCC values, most likely because fewer channels associated with non-resonant processes were included in the QMOCC calculations.

Calculations of the impact-parameter and close-coupling (IPCC) performed by Sakabe *et al.*[10] are close to the measurements of Daley *et al.*[7] but fail to reproduce the characteristic oscillatory structures in the overlapping energy region. Although the results of IPCC closely follow the trend of the present results in the low-energy region, the cross sections are approximately 13% smaller than those reported in this work and measurements of Rutherford *et al.*[9] The results obtained using the impact parameter treatment based on the Firsov model (IPTF) by Copeland *et al.*[11] also show a similar energy dependence to the present calculations. However, their cross sections significantly deviate from other theoretical predictions, being about 30%–50% smaller than the present results. These discrepancies may result from the use of the semi-empirical method proposed by Firsov[31] to describe symmetric resonant single-charge transfer in the calculations of Copeland *et al.*[11]

In the energy range of 6.2–87 eV/amu, the results reported by Bukhteev *et al.*[6] are approximately half of those obtained in the present work. The deviation between our calculations and the experimental data measured by Daley *et al.*[7] remains within 25%. The differences may be attributed to the fact that the previous measurements are relative cross sections. Starting from an energy of approximately 300 eV/amu, an oscillatory structure in the present resonant charge transfer cross section becomes evident, with the amplitude increasing as the impact energy rises. But the oscillatory behaviors obtained from the present QMOCC and Sakabe *et al.*[10] are out of phase with measurements of Daley *et al.*[7] The oscillatory structure in resonant charge-transfer cross sections arises from interference effects associated with extrema in the difference potential between the gerade and ungerade states. When this potential exhibits an extremum at a specific internuclear distance, interference between scattering amplitudes leads to periodic modulations in the cross section. The frequency is determined by the extremum position, while the amplitude reflects the magnitude and phase of the potential difference.[32–34]

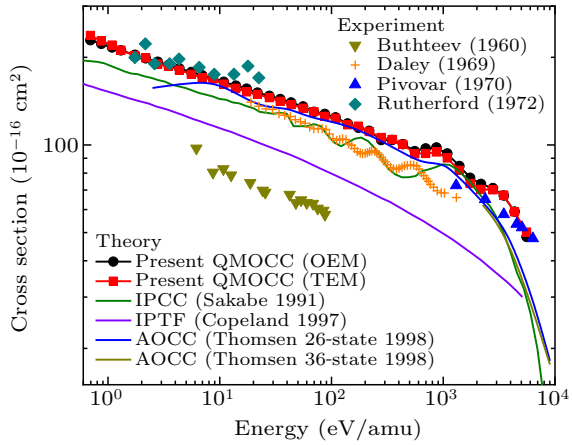


Fig. 4. Comparison of present resonant charge transfer cross sections with other theoretical and experimental results. Theories: present QMOCC single-electron model (black solid line with filled circles) and thirteen-electron model (red solid line with filled squares), impact-parameter and close-coupling (IPCC) methods of Sakabe *et al.*[10] (green solid line), impact parameter and treatment of Firsov (IPTF) method of Copeland *et al.*[11] (violet solid line), atomic orbital close-coupling (AOCC) of Thomsen *et al.*[12] (26 states: blue solid line, 36 states: dark yellow solid line). Experiments: Rutherford *et al.*[9] (filled rhombuses), Pivovar *et al.*[8] (filled triangles), Bukhteev *et al.*[6] (filled inverted triangles), Daley *et al.*[7] (crosses).

3.2.2. Non-resonant charge transfer

3.2.2.1. State-selected cross sections

In addition to the resonant charge transfer process, in which electrons in the 3s orbital of the target Na atoms are captured into the same orbital of the incident Na^+ ions. Electrons in the 3s orbital can also be transferred to the excited states of Na^+; these processes are referred to as non-resonant charge transfer in the present study. The primary non-resonant state-selective cross sections for electron capture into Na[($2p^6$)3p, 3d, 4s, 4p] states are presented in Fig. 5 from 0.2 eV/amu to 5600 eV/amu, calculated using the QMOCC method with OEM and TEM models. The resonant charge transfer cross sections are significantly larger than those of the non-resonant processes within the energy range considered in this study. Moreover, as the collision energy increases, the cross sections for non-resonant charge transfer gradually increase, while those for resonant charge transfer show a decreasing trend. This behavior can be reasonably explained by the fact that resonant electron transfer at low collision velocities requires almost no energy exchange from the relative nuclear motion to the electronic motion. The collision system can be effectively described as a quasi-diatomic molecule with a time-dependent internuclear separation, where the electron dynamics are perturbed by the nuclear motion.[35]

As shown in Fig. 5, electron capture predominantly occurs into the Na($2p^6 3p$) state in our calculations, which can be attributed to the small energy gap (2.1 eV) and the long-range Demkov-type coupling with the initial state. At collision energies below 30 eV/amu, the cross sections for capture into the 3p state are significantly larger than those for other states. However, when the collision energy exceeds 30 eV/amu, the cross sections for different final states become comparable in magnitude. This behavior is due to the opening of channels corresponding to higher excited states at higher collision energies, where the associated radial coupling matrix elements begin to play a significant role. As mentioned above, the cross sections are highly sensitive to the molecular structure in the low-energy region. When the values of cross section are relatively small, the small difference between matrix elements and potential energy curves obtained from the OEM and TEM calculations will lead to obvious differences. In addition, the finite-difference method employed in the radial coupling calculations would also introduce discrepancies for small values of cross sections.

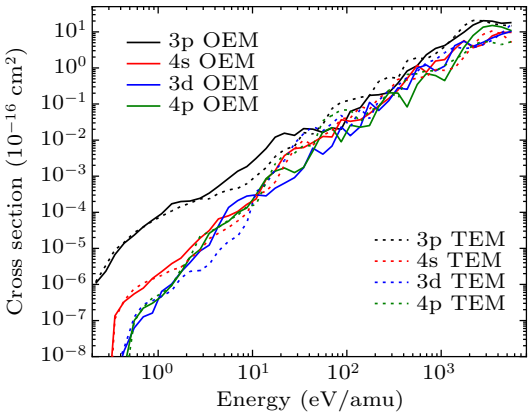


Fig. 5. The present non-resonant state-selective cross sections for electron capture to Na($2p^6 nl$, $n \leq 4$) states. Solid lines: single-electron model (OEM); dashed lines: thirteen-electron model (TEM).

3.2.2.2. Total cross section

By summing over the state-selective cross sections, the total non-resonant charge transfer cross sections for both the OEM and TEM models are obtained, as illustrated in Fig. 6. The values of total non-resonant cross sections vary from approximately 1×10^{-22} cm^2 to 5×10^{-15} cm^2 as the collision energy increases from 0.2 to 5600 eV/amu. It can be observed that at low collision energies, the total non-resonant cross sections are extremely small, indicating that non-resonant processes are strongly suppressed in this regime. However, with increasing collision energy, the cross sections rise rapidly. This sharp increase is attributed to the opening of additional non-resonant channels and the enhanced contributions of higher excited states. When the collision energy exceeds approximately 3000 eV/amu, the non-resonant cross sections become comparable to those of the resonant charge transfer processes, reaching the same order of magnitude. This trend suggests that at sufficiently high energies, non-resonant channels play a non-negligible role and may even compete with the resonant pathways in determining the overall charge transfer dynamics. To the best of our knowledge, no theoretical calculations or experimental measurements of the non-resonant state-selective charge transfer cross sections in this specific collision system have been reported to date. Therefore, the present results not only provide the first theoretical predictions for these processes but also offer valuable reference data for future experimental investigations and further theoretical developments in the field of ion–atom collision dynamics.

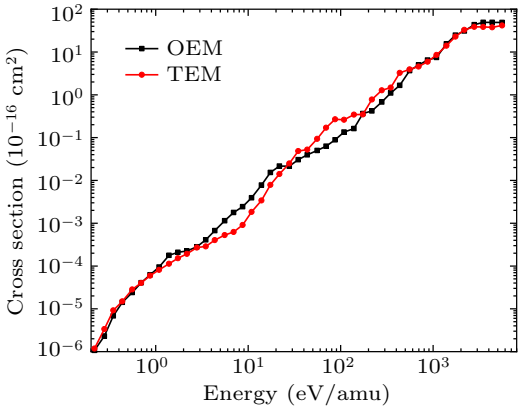


Fig. 6. Total non-resonant charge-transfer cross sections calculated using the one-electron model and the thirteen-electron model.

4. Conclusion

In this work, a comprehensive theoretical investigation of both resonant and non-resonant charge transfer processes in the homonuclear $Na^+ + Na(3s)$ collision system has been conducted using the fully quantum-mechanical molecular orbital close-coupling (QMOCC) method. The electronic structures were calculated using the MRD-CI method under both the one-electron model (OEM) and the thirteen-electron model (TEM), with careful consideration of the electron translation factors (ETFs) in the radial/rotational couplings. For resonant charge transfer, the calculated cross sections exhibit excellent agreement with previous results of Thomsen *et al.*,[12] Pivovar *et al.*[8] and Rutherford *et al.*[9] The oscillations observed in the present work are attributed to the non-monotonic behavior of the potential energy differences between the gerade and ungerade states. Further theoretical investigations are required to reconcile the phase of these oscillatory structures with the experimental cross sections reported by Daley *et al.*[7] The non-resonant charge transfer processes, including state-selective and total cross sections for capture into low-lying excited states of Na^+ ($n \leq 4$), were also systematically examined. It is found that electron capture predominantly occurs into the 3p state at low energies, while contributions from other channels become comparable at higher energies. The total non-resonant cross section rises rapidly with increasing energy, reaching magnitudes comparable to those of resonant

transfer. These results not only provide the first set of theoretical predictions for non-resonant processes in this system but also offer essential data for future benchmarking studies. Overall, the present study significantly advances the understanding of charge transfer dynamics in symmetric ion-atom collisions, and the reported results serve as a valuable foundation for further theoretical developments and experimental validations in the field.

Acknowledgement

This paper was supported by the National Natural Science Foundation of China (Grant Nos. 11774344, 12204288, and 12504293).

References

[1] Fan Y X, Xing D D, Cui S C, Wang X X, Ran J X, Lin K Z, Zhu X B, Zhao D M, Guo D L, Gao Y, Zhang S F, Zhu X L and Ma X W 2025 *Chin. Phys. B* **34** 073402
[2] Levandier D J, Dressler R A, Williams S and Murad E 1997 *J. Chem. Soc. Faraday Trans.* **93** 2611
[3] Stangeby P C 2000 *Plasma Phys. Control. Fusion* **43** 223
[4] Mashonkina L I, Shimanskii V V and Sakhibullin N A 2000 *Astron. Rep.* **44** 790
[5] Brown R A and Schneider N M 1981 *Icarus* **48** 519
[6] Bukhteev A M and Bydin Y F 1960 *Izv. Akad. Nauk SSSR Ser. Fiz* **24** 964
[7] Daley H L and Perel J 6*th Int. Conf. on the Physics of Electronic and Atomic Collisions*, Cambridge, p. 1051
[8] Pivovar L I, Nikolaichuk L I and Grigor'Ev A N 1969 *Sov. Phys. JETP* **30** 236
[9] Rutherford J A, Mathis R F, Turner B R and Vroom D A 1972 *J. Chem. Phys.* **56** 4654
[10] Sakabe S and Izawa Y 1991 *Atom. Data Nucl. Data* **49** 257
[11] Copeland F B M and Crothers D S F 1997 *Atom. Data Nucl. Data* **65** 273
[12] Thomsen J W, Andersen N, Campbell E E B, Hertel I V and Nielsen S E 1998 *J. Phys. B: At. Mol. Opt. Phys.* **31** 3429
[13] Buenker R J and Phillips R A 1985 *J. Mol. Struct.: Theochem* **123** 291
[14] Krebs S and Buenker R J 1995 *J. Chem. Phys.* **103** 5613
[15] Wang K, Qu Y Z, Liu C H, Liu L, Wu Y, Liebermann H P and Buenker R J 2020 *Chin. Phys. B* **29** 093401
[16] Errea L F, Mendez L and Riera A 1982 *J. Phys. B: At. Mol. Phys.* **15** 101
[17] Kimura M and Lane N F 1989 *Adv. At. Mol. Opt. Phys.* **26** 79
[18] Wang J G, He B, Ning Y, Liu C L, Yan J, Stancil P C and Schultz D R 2006 *Phys. Rev. A* **74** 052709
[19] Zygelman B, Cooper D L, Ford M J, Dalgarno A, Gerratt J and Raimondi M 1992 *Phys. Rev. A* **46** 3846
[20] Heil T G, Butler S E and Dalgarno A 1981 *Phys. Rev. A* **23** 1100
[21] Bransden B H and McDowell M R C 1992 *Charge Exchange and the Theory of Ion-Atom Collision* (Oxford: Clarendon Press) pp. 300–301
[22] Johnson B R 1973 *J. Comput. Phys.* **13** 445
[23] Pritchard B P, Altarawy D, Didier B, Gibson T D and Windus T L 2019 *J. Chem Inf. Model.* **59** 4814
[24] Schuchardt K L, Didier B T, Elsethagen T, Sun L, Gurumoorthi V, Chase J, Li J and Windus T L 2007 *J. Chem Inf. Model.* **47** 1045
[25] Fernandez Pacios L and Christiansen P A 1985 *J. Chem. Phys.* **82** 2664
[26] Kramida A, Ralchenko Y, Reader J and NIST ASD Team 2019 *NIST Atomic Spectra Database* (National Institute of Standards and Technology, Gaithersburg, MD)
[27] Kimura M and Lane N F 1990 *Phys. Rev. A* **41** 5938
[28] Liu C H, Liu L, Qu Y Z, Wang J G and Janev R K 2010 *Phys. Rev. A* **82** 022710
[29] Olson R E 1970 *Phys. Rev. A* **2** 121
[30] Errea L F, Harel C, Jouin H, Mhdez L, Pons B and Riera A 1994 *J. Phys. B: At. Mol. Opt. Phys.* **27** 3603
[31] Firsov O B 1951 *Sov. Phys. JETP* **21** 1001
[32] Smith F J 1966 *Phys. Lett.* **20** 271
[33] Perel J, Daley H L, Peek J M and Green T A 1969 *Phys. Rev. Lett.* **23** 677
[34] Perel J 1970 *Phys. Rev. A* **1** 369
[35] Fritsch W and Lin C D 1991 *Phys. Rep.* **202** 1